UC 408
LBL-29150

Lawrence Berkeley Laboratory
UNIVERSITY OF CALIFORNIA

Engineering Division

To be presented at the SPIE 1990 International Symposium on Optical and Optoelectronic Applied Science and Engineering, San Diego, CA, July 9–13, 1990, and to be published in the Proceedings

Characteristics of Feasible Images Obtained from Real PET Data by MLE, Bayesian and Sieve Methods

J. Llacer and A.C. Bajamonde

For Reference

Not to be taken from this room

June 1990

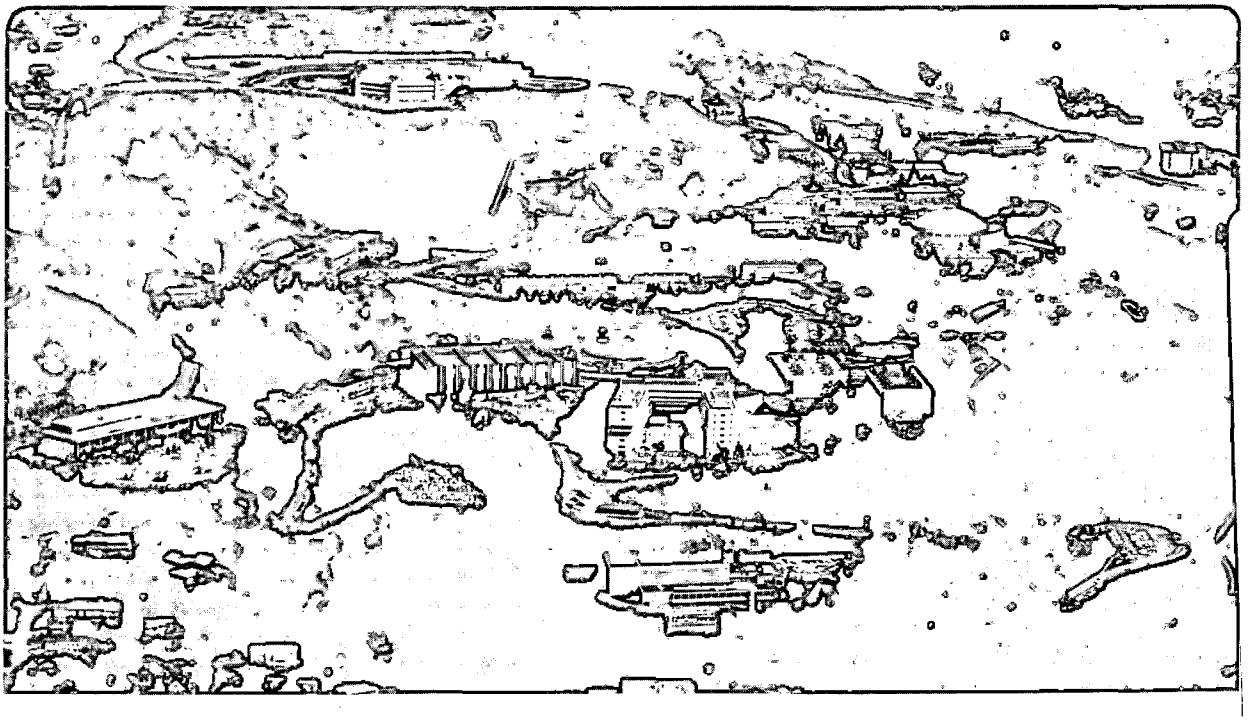

Prepared for the U.S. Department of Energy under Contract Number DE-AC03-76SF00098.

LBL-29150
Copy 1
Bldg. 50 Library.

DISCLAIMER

This document was prepared as an account of work sponsored by the United States Government. While this document is believed to contain correct information, neither the United States Government nor any agency thereof, nor the Regents of the University of California, nor any of their employees, makes any warranty, express or implied, or assumes any legal responsibility for the accuracy, completeness, or usefulness of any information, apparatus, product, or process disclosed, or represents that its use would not infringe privately owned rights. Reference herein to any specific commercial product, process, or service by its trade name, trademark, manufacturer, or otherwise, does not necessarily constitute or imply its endorsement, recommendation, or favoring by the United States Government or any agency thereof, or the Regents of the University of California. The views and opinions of authors expressed herein do not necessarily state or reflect those of the United States Government or any agency thereof or the Regents of the University of California.

LBL-29150

Characteristics of feasible images obtained from real PET data by MLE, Bayesian and sieve methods

Jorge Llacer and Alex C. Bajamonde*

Engineering Division, Lawrence Berkeley Laboratory
and *Department of Statistics
University of California, Berkeley, CA 94720

This work has been supported, in part, by a grant from the National Institutes of Health, CA-39501 and by the Director, Office of Energy Research, Office of Health and Environmental Research, Physical and Technological Division, of the U.S. Department of Energy under Contract No. DE-AC03-76SF00098.

LBL-29150

Characteristics of feasible images obtained from real PET data by MLE, Bayesian and sieve methods

Jorge Llacer and Alex C. Bajamonde*

Engineering Division, Lawrence Berkeley Laboratory
and *Department of Statistics
University of California, Berkeley, CA 94720

ABSTRACT

The frequency spectral characteristics, bias and variance of images reconstructed from real Positron Emission Tomography (PET) data have been studied. Feasible images obtained from statistically based reconstruction methods have been compared to Filtered Backprojection (FBP) images. Feasible images have been described as those images that are compatible with the measured data by consideration of the Poisson nature of the emission process. The results show that the spectral characteristics of reconstructions obtained by statistically based methods are at least as good as those obtained by the FBP methods. With some exceptions, statistically based reconstructions do not exhibit abnormal amounts of bias. The most significant difference between the two groups of reconstructions is in the image variance, where the statistically based methods yield substantially smaller variances in the regions with smaller image intensity than the FBP images.

1. INTRODUCTION

Maximum Likelihood Estimator (MLE), Bayesian methods with a variety of prior distributions and the method of sieves are being investigated as methods for reconstructing Emission Tomography (ET) images at a number of institutions. The number of publications reporting theoretical and experimental results in those areas of work is already too large to reference here. Although there is general agreement that the images recovered by those statistically based methods are "superior" to Filtered Backprojection (FBP) images, there appears to be little that is specifically known on what that superiority consists in. In this paper we shall report the results of an extensive analysis of three main groups of variables that can characterize images: their frequency spectrum, bias and variance.

We take for granted that statistically based reconstruction methods can incorporate in the transition matrix space variant point spread functions, "missing cones" of projection data, corrections for absorption and detector gains, Compton scattering in the detectors and the consequent crystal penetration, lack of collinearity of the two annihilation γ-rays in Positron Emission Tomography (PET), etc., and that the incorporation of those factors into the transition matrix represents a practical advantage over FBP methods of reconstruction. The more fundamental benefit of statistically based reconstruction methods should stem, however, from the fact that the correct Poisson distribution that governs radioactive disintegration is used to define the target function to be maximized by the reconstruction algorithms. FBP methods implicitly assume that distribution is Gaussian with a single, unspecified, standard deviation.[1] We shall show that, for the methods investigated in the present work, the principal advantage of the statistical methods appears due to the utilization of the Poisson distribution, although we do not have a proof.

In the selection of images reconstructed by statistically based methods we have chosen feasible images exclusively. It is well known that the MLE method, as implemented, for example, from the EM algorithm by Shepp and Vardi,[2] yields unacceptably noisy images if the iterative process is allowed to continue past a certain number of iterations. Llacer and Veklerov[3] have described feasible images as those images that, if they were a radiation field, could have generated the initial projection data by the Poisson process that governs radioactive decay. Formal definitions of feasibility, as well as a practical test that has been used in the work reported in this paper can be found in Ref. 3. This paper will first describe the selection of data and of filters for the FBP reconstructions, the selection of methods and parameters for the statistically based reconstructions, will show and evaluate the image frequency spectra of the various groups of images, will give a practical definition of bias for PET images, and show representative results of bias and variance analysis.

2. SELECTION OF DATA AND RECONSTRUCTION METHODS

2.1 Selection of data

Statistically based methods of reconstruction depend on the specification of a transition matrix whose elements contain probabilities that γ-rays emitted from a specific pixel will be detected by a specific detector "tube". A tube can be defined by a particular collimator hole in Single Photon Emission Tomography (SPET) or a pair of detectors in Positron Emission Tomography (PET), for example. In computer simulation studies the characteristics of that transition matrix can be made identical to the actual probabilities of γ-ray emission, but in practice the transition matrix can only be approximated. Monte Carlo methods can be used to calculate useful approximations to the true transition matrix, as has been done by Llacer et al. [4,5] for small positron emission cameras, by Floyd et al.[6] for SPET and by Veklerov et al.[7] for PET. It has been found, however, that even Monte Carlo approximations can be sufficiently different from the real instrument transition matrices that strict tests for image feasibility fail unless they are relaxed by the introduction of an adjustable parameter that quantifies the accuracy with which the transition matrix is known.[3]

Because of the expected inaccuracy of transition matrices, we decided that the current study of image characteristics should be based on real PET data, so that the comparison of imaging algorithms is carried out closer to what clinical practice is likely to encounter. PET data of the Hoffman brain phantom[8] from the ECAT-III instrument that was in use at the UCLA School of Medicine were obtained for this study. That brain phantom mimics Fluoro-dioxi-glucose (FDG) brain studies, which constitute the most common application of PET in a clinical setting. FDG studies may not be, however, those that benefit most from statistically based algorithms, as will be discussed below.

One set of projection data with 55 million (55M) counts was obtained as a reference and ten sets with 1 million (1M) counts each were obtained as independent data sets. The number of counts in the latter sets was selected as representative of typical brain studies with the ECAT-III. Figure 1 shows the outline of the Hoffman brain phantom. The ratio of activities between the regions in black and those in white in the interior of the phantom is approximately 4.5:1. Although the activity ratio in the phantom can be controlled quite accurately, the actual ratio measured by the tomograph is not well known due to different solid angles seen by the detector crystals from different positions in the imaging plane. This will impose a serious limitation when attempting to measure bias in the images, as will be discussed below.

Fig. 1: Outline of the Hoffman brain phantom.

The data for the reconstructions were corrected for background by the standard method of subtracting an estimate obtained by delayed coincidences in the PET instrument, with negative counts set to zero. With less than 5% background counts, this results in a small distortion to the Poisson distribution of the original projection data. The ECAT-III instrument has a sampling distance of 3.05 mm at the center of the field. Reconstructions were carried out in a 128 x 128 grid with pixel dimensions of 2.033 x 2.033 mm.

2.2 Filtered Backprojection methods

All the filtered backprojection reconstructions were carried out using algorithms from the RECLBL library.[9] The backprojector BIN, that allows the use of different projection bin and pixel sizes, was used for all the reconstructions. A full bandwidth Shepp-Logan filter in configuration space was used for the reconstructions with identifier "sl". The rest of the FBP reconstructions were carried out by filtering in frequency domain. The filter types and parameters used are described in Table I. Filter "slf1" corresponds to the filter that radiologists at the UCLA School of Medicine have found empirically to give the most useful clinical information for brain images with 1M counts. Both the "slf1" and "slf2" filters are not part of the RECLBL library but were synthesized for the current study. The parameters for the Butterworth filter "bw0", which is part of that library and allows non-integer filter orders,[10] were selected by the method described in Ref. 9 to enhance slightly the intermediate frequency part of the pass band over the "slf1" filter, but cutting a substantial part of the higher frequency noise. Figure 2 shows the filter functions for the "slf1" and "bw0" filters.

TABLE I - Parameters for FBP reconstructions		
Identifier	Filter	Parameters
ramp	Ramp, freq. domain	
sl	Shepp-Logan, conf. space	
slf1	Shepp-Logan, freq. domain	$f_c = 0.65$ Hz/cm
slf2	ditto	$f_c = 0.57$ Hz/cm
bw0	Butterworth, freq. domain	$f_p = 0.82$, $f_s = 1.64$ Hz/cm

2.3 Statistically based reconstructions

As indicated above, feasible or nearly feasible images have been used for the statistically based reconstructions. Using the methods described in Ref. 3 for the feasibility tests, a number of reconstruction methods have been investigated. The MLE method described in Ref. 2 has been used in two different forms: 1) "simple MLE", in which absorption and detector gain corrections were used to multiply the original projection data before reconstruction, and 2) "asymmetric MLE" in which the corrections are used to modify the transition matrix elements in a more strict adherence to the definition of such a matrix. This method, in effect, breaks up the 8-fold symmetry of the transition matrix, a characteristic that we use to reduce the amount of storage for that matrix, but preserves the Poisson or near-Poisson nature of the projection data. For the 1M counts data sets, both methods of reconstruction were carried to 30 iterations, where our tests indicated the onset of feasiblity of the recovered image. Feasible images were also obtained by carrying out the above iterative procedures to 50 iterations, where the images are beginning to leave the feasibility region, signaled by an increase of the noise level in the high activity regions, and filtering back to feasibility with a Gaussian filter.[11] For the 55M count reference data set, the number of iterations to feasibility was higher, as will be shown below. A Maximum a Posteriori method (FMAPE) with entropy prior[12] has also been used to recover feasible images. The Bayesian algorithm seeks to obtain an image that maximizes a product of entropy and likelihood, with one weight parameter (Δa) that can be adjusted for convergence to feasible images. Finally, the method of sieves[13] has been used to obtain feasible images by adjustment of the sieve and resolution kernels to yield noise-free images that converged to feasible or nearly feasible images.

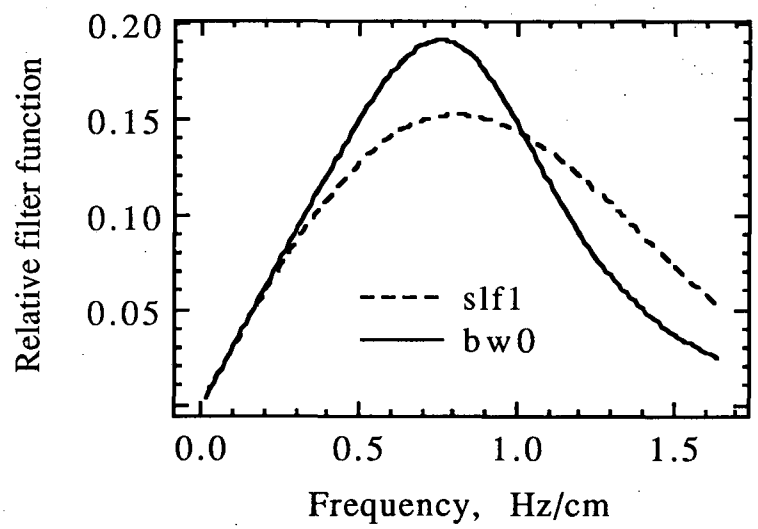

Fig. 2: Relative response of the Shepp-Logan filter "slf1" and the Butterworth filter "bw0".

The values of the sieve and resolution kernels were chosen after a search for parameter values yielding feasible images was made.[14] The strictly feasible images obtained tended to be excessively noisy (note that we consider feasibility a necessary condition for an image, but not a sufficient condition). The sieve images obtained with the parameters of Table II were very close to being feasible, having a slightly oversmoothed appearance.

Table II - Parameters for statistically based reconstructions		
Identifier	Method	Parameters
30	Simple MLE, 30 its.	
50_0.7	ditto, 50 its.	Post filtering σ = 1.42 mm (0.7 pixels)
a_30	Asymmetric MLE, 30 its.	
a_50_0.7	ditto, 50 its.	Post filtering σ = 1.42 mm (0.7 pixels)
bbg_150_0.5	FMAPE, 150 its.	Δa = 900, post filtering σ = 1.01 mm
s1	sieves, 300 its.	σ_s = 1.83, σ_r = 1.83 mm
s2	ditto	σ_s = 2.23, σ_r = 0.93 mm
s3	ditto	σ_s = 2.23, σ_r = 1.62 mm

3. IMAGE FREQUENCY SPECTRA

We use a standard definition of Image Frequency Spectrum (IFS): the magnitude of the 2-dimensional Fourier transform of an image. We avoid the use of the term Power Spectral Density, or Spectral Density, because this term is more properly reserved for the Fourier transform of the autocorrelation function of a stationary, or quasi-stationary random process. Reconstructed images from a single phantom have a random (noise) part and a deterministic (image) part and are not stationary. In this study we will compare the frequency spectrum of a reference image (55M counts) reconstructed with the "sl" filter to the spectra of images reconstructed by various methods. The emphasis is in obtaining the frequency spectrum of the deterministic (image) part of the reconstructions, to see how well image features are treated by each method. Using the "sl" filter for the reference image results in an image with excellent feature contents and somewhat lower noise than with the ramp filter. The "sl" filter also avoids the characteristic "ringing" of the latter filter. Figure 3 shows the reference image.

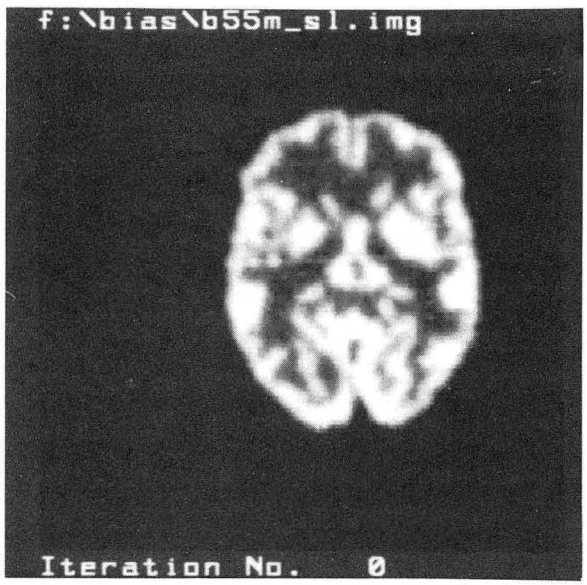

XBB 906-4730

Fig. 3: Reference FBP image from a 55 million count data set. Shepp-Logan filter in configuration space.

For a linear method of reconstruction, one could emphasize the image features by adding the ten independent projection data sets, carrying out one single reconstruction and then obtaining the IFS. For the non-linear statistical methods of reconstruction, we have no assurance that the results of that study would be equivalent to carrying out ten separate reconstructions, adding up the images and then obtaining the IFS. For that reason we have carried out the IFS study by the latter method, except where noted, which is correct for both linear and non-linear methods of reconstruction.

The 2-dimensional IFS's are not convenient to present in a printed form. It appears sufficient to examine one-dimensional cuts through the two-dimensional spectra. The x-frequency axis will therefore be shown for all the images to be described in this section.

Figure 4 shows the IFS of the reference image in comparison with those of 4 independent 1M images, also reconstructed by the "sl" filter. It is apparent that image features are beginning to be obscured by noise in the 1M reconstructions at frequencies above approximately 0.8 Hz/cm. We do not know up to what frequency the 55M image conveys image features, but we can expect those features to be present up to frequencies above the onset of noise in the 1M images. The empirical choice of the "slf1" filter by the users of ECAT-III brain images at UCLA is then consistent with the above finding, as seen from Fig. 2. The choice of the "bw0" filter is also well justified. It will reconstruct better image features at the edge of the region where noise becomes dominant, and it cuts off more rapidly than the "slf1" filter at higher frequencies.

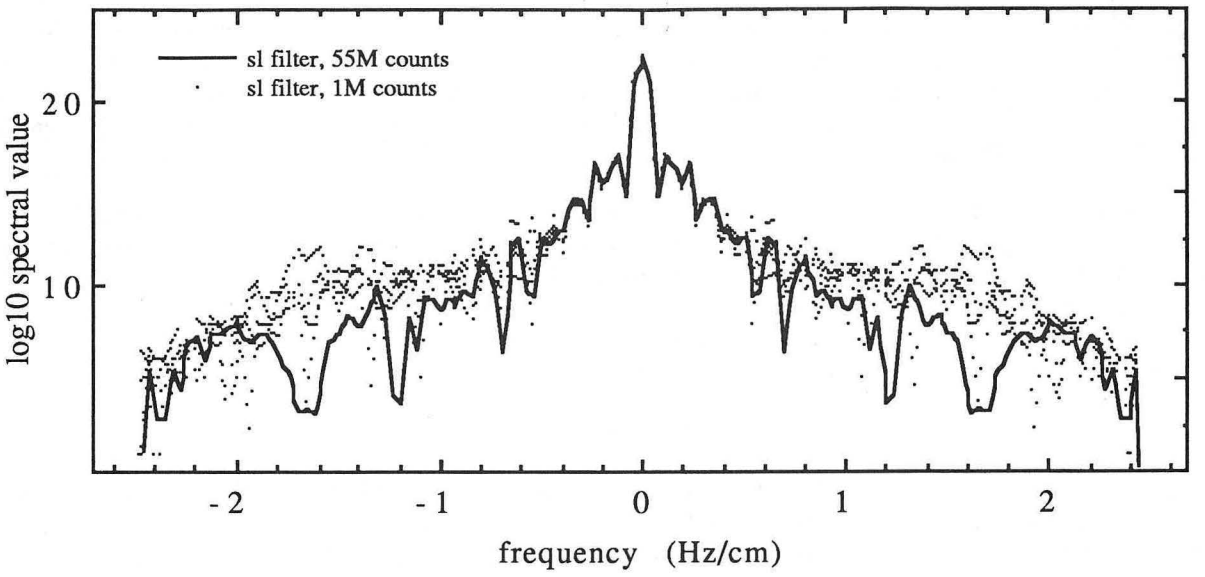

Fig. 4: Comparison of the IFS's of the reference image with four independent 1M images, showing the region of frequencies over which the 1M images convey source features.

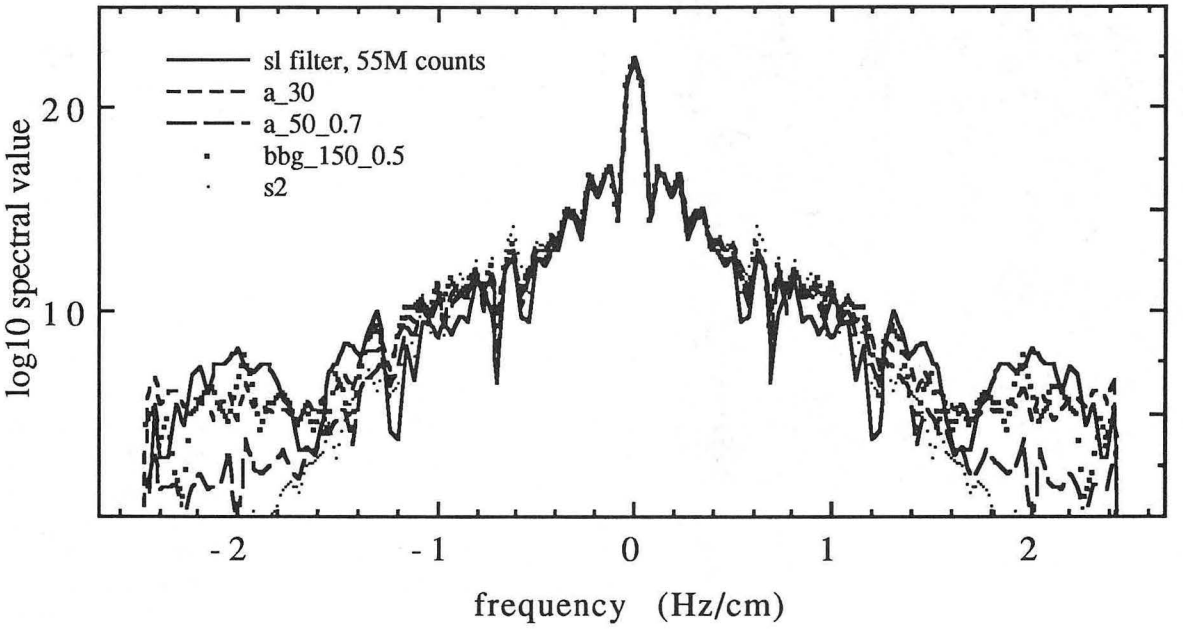

Fig. 5: Comparison of the IFS's of the reference image with feasible images reconstructed by some of the methods and parameters of Table II.

The "simple MLE" and the "asymmetric MLE" reconstructions do not show any significant differences in behavior in the frequency domain and only the latter reconstructions results are shown here. Figure 5 shows a comparison of the IFS of the reference image with the IFS's of feasible reconstructions by the different statistically based reconstruction methods. The most significant difference is in a noticeable increase of the spectra of the feasible images between 0.7 and 1.2 Hz/cm with respect to the reference. This may account for the apparent higher sharpness of MLE reconstructions when compared to FBP results filtered to a similar noise level.

The results of Fig. 5 can be summarized by indicating that frequency spectra of feasible images exhibit strong similarities, independent of the reconstruction method. Those methods that use a final filtering operation, including the method of sieves, show a decreased spectrum at the high frequencies, where reconstruction noise would be dominant at 1M counts. An increase in image sharpness with respect to the reference FBP image is also noticed at the intermediate frequencies. These observations are consistent with an examination of images and do not seem to favor any specific method of statistically based image reconstruction over the others.

4. BIAS ANALYSIS

Bias has a well defined meaning in Statistics and, in the imaging context, could be described as differences between the expected value of reconstructed pixel intensities and the correct values. In the case of tomographic reconstructions, in which filtering of high frequencies is a necessity, the above definition of bias is not practical, since all edges in the image would show bias. A more practical definition can be devised as the difference between the expected average value in extended uniform regions, away from edges, and the correct average values for those regions.

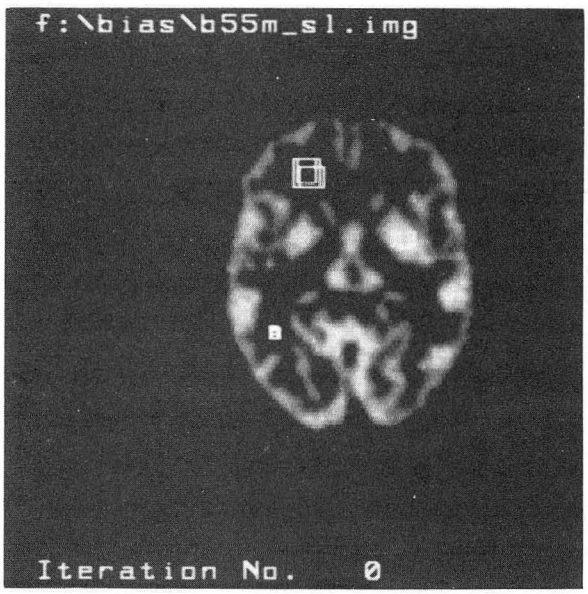

XBB 906-4731

Fig. 6: Hoffman brain phantom image, showing the 9 ROI's obtained from three main areas for bias analysis.

The Hoffman brain phantom has been designed with two levels of activity, simulating grey and white matter. Regions corresponding to the two levels can be used to define ratios of activities which the reconstructed images should reproduce accurately. In the present study, as indicated earlier, the correct ratios seen by the tomographic instrument are not well known, except that they should be in the vicinity of 4.5:1. As a consequence, we do not have an accurate way of assessing the bias caused by the different reconstruction methods. It should be mentioned that reconstructions carried out by both FBP and statistical methods with data generated by computer simulation and reconstructed with exact transition matrices have been found to show no significant bias.

In spite of the difficulties just indicated, it has been possible to carry out an approximate bias analysis which allows us to draw some interesting conclusions. Figure 6 shows the Hoffman brain phantom with 3 main areas: a1 placed in the hot large region shown, a2 in the cool large white matter area and a3 in the narrow cool white matter area. Each of the three main areas has been sampled in three different manners, by generating slightly different regions-of-interest (ROI's) to encompass in one case some neighboring pixels that were not considered in another case. The resulting 9 ROI's are shown in Figure 6. The generation of 3 ROI's from each main area allows to estimate the variability of the measurement caused by setting specific limits to the ROI.

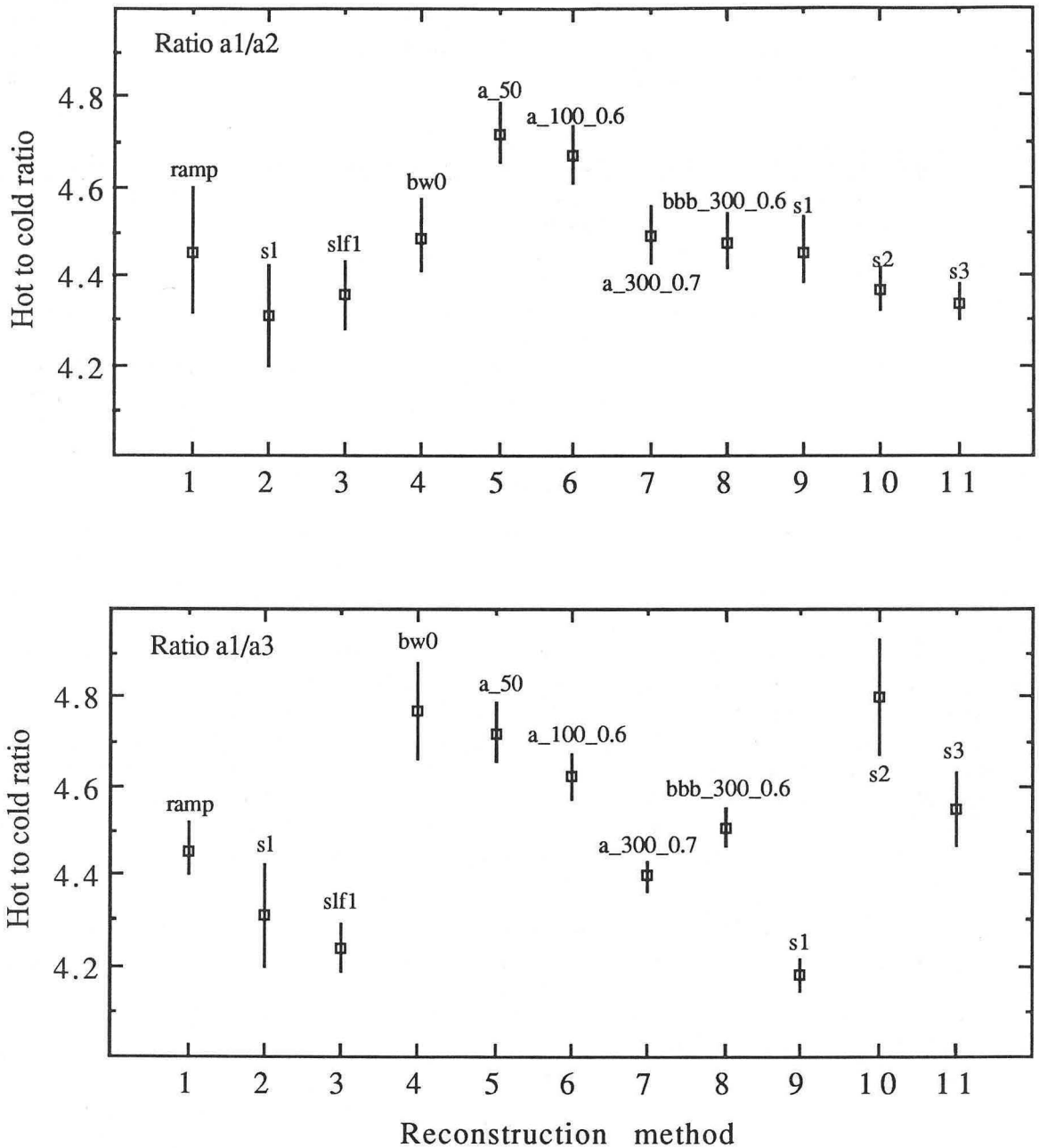

Fig. 7: Mean and standard deviation of the ratios of hot/cold regions for reconstruction methods and parameters of Table III. Top: Hot/large cold region (a1/a2); Bottom: Hot/narrow cold region (a1/a3).

For each method of reconstruction, nine different activity ratios can be obtained by dividing the average activity in the ROI's at a1 by those at a2, and nine more ratios can be obtained by dividing the activities at a1 by those at a3. The mean and standard deviation of each group of 9 ratios has been obtained and is shown in Fig. 7. In order to decrease the effect of noise as much as possible in this study, the reference 55M count data set was used exclusively. The different methods and parameters shown in Table III were used for the reconstructions.

The ratios for the larger regions a1/a2 are all different from each other, and the only meaningful observation that can be made is that, in the asymmetric MLE reconstructions (as in the Simple MLE not shown), the values of the ratios at iterations corresponding to the onset of feasibility (50 to 100 its. for 55M counts) have not reached their final values. At iteration 300 and beyond, the ratio a1/a2 does not differ substantially from those obtained by other methods of reconstruction.

Table III - Methods and parameters used for bias analysis, 55 M count data set

Identifier	Method	Parameters
ramp	FBP - Ramp filter	
sl	FBP - Shepp-Logan, config. space	
slf1	FBP - Shepp-Logan, freq. domain	$f_c = 0.65$ Hz/cm
bw0	FBP - Butterworth, freq. domain	$f_p = 0.82$, $f_s = 1.64$ Hz/cm
a_50	Asymmetric MLE, 50 its.	
a_100_0.6	ditto, 100 its.	Post filtering, $\sigma = 1.23$ mm
a_300_0.7	ditto, 300 its.	Post filtering, $\sigma = 1.42$ mm
bbb_300_0.6	FMAPE, 300 its.	Post filtering, $\sigma = 1.23$ mm
s1	sieves, 1000 its.	$\sigma_s = 1.83$, $\sigma_r = 1.83$ mm
s2	sieves, 500 its.	$\sigma_s = 2.23$, $\sigma_r = 0.93$ mm
s3	ditto	$\sigma_s = 2.23$, $\sigma_r = 1.62$ mm

The situation for the ratios of regions a1/a3 in the Asymmetric MLE reconstructions is the same as above, but in addition, other effects can be noticed in other reconstructions. Region a3, being a narrow valley between high intensity regions, can be expected to be sensitive to excessive smoothing and to "ringing". In going from the ramp reconstruction to the sl and further to the slf1, the reduction of the ratio indicates that the smoothing caused by filtering with lower bandpass affects the image values at the valley a3. The bw0 results with the Butterworth filter, as well as the s2 results with the sieve method show the opposite effect: there is an exaggeration in the depth of the narrow valley. This "ringing" effect can be expected from the Butterworth filter when its high frequency response drops too rapidly. This effect is particularly noticeable if the ratio f_s/f_p of the filter is made smaller than approximately 2.0, making the filter order larger than approximately 6.0. Ringing is also seen in sieve reconstructions when the difference between the sieve kernel and resolution kernel parameters is too high. The ratio for the s3 reconstruction is closer to the ramp results, for example, than that of s2. The low value of the a1/a3 ratio for the s1 reconstruction is not understood at this time.

A preliminary conclusion from the limited bias study is, then, that the use of a Butterworth filter for FBP reconstructions, as well as sieves for a statistically based method has to be considered carefully. A "ringing" image will have a very attractive appearance as long as the effect is not excessive, but image values may be in error in narrow regions, hot or cold. A second point that can be made is that MLE reconstructions stopped at the onset of feasibility have not yet attained the final value of activity in all their regions. It is preferable to iterate past the onset of feasibility, when the image begins to become noisy and filter back to feasibility with a small Gaussian kernel.

5. VARIANCE ANALYSIS

The pixel-by-pixel variance of reconstructions from 10 independent 1M count data sets has been examined for the FBP and statistical methods discussed above. The process has been carried out in the following steps:

1) The reference 55M count data set has been reconstructed by the "sl" method and a histogram of number of pixels having a certain number of counts vs. number of counts in a pixel has been constructed. The histogram is shown in Fig. 8 for the pixels inside the perimeter of the brain phantom. For example, there were approximately 25 pixels that contained 40,000 counts.

2) All the pixels in the brain phantom image were classified into three regions and labels were affixed to each pixel for:

a) High intensity pixels, i.e., having more than 30,000 counts/pixel.
b) Low intensity pixels within the brain, i.e., having between 10,000 and 20,000 counts/pixel, and
c) All low intensity pixels, within and outside the brain, i.e., from 0 - 20,000 counts/pixel in the 55M count image.

3) The ten independent data sets were reconstructed by the different methods and parameters of Table III.

4) The pixel-by-pixel means and standard deviations for each ensemble of 10 images were calculated, separating the pixels according to the classification of 2), and

5) Histograms of number of pixels having a certain value of Standard Deviacion (SD) vs. SD were made for each of the classifications of 2) and each method of reconstruction.

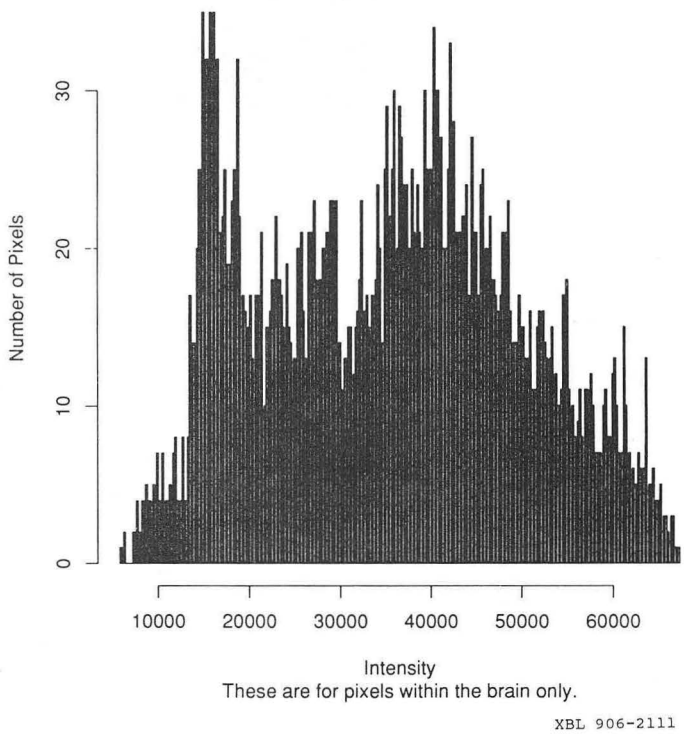

Fig. 8: Histogram of number of pixels vs. pixel intensity (counts) for the 55M reference image.

The obtained results can be classified into two main groups: FBP images and statistically based images, with small variations within each group depending on filtering, number of iterations and somewhat depending on the actual reconstruction method. The results for the 10 independent images reconstructed by FBP, using the slf1 filter and the asymmetric MLE at iteration 30, soon after the onset of feasibility, will be shown as representative of the two groups of results.

Figure 9 shows the FBP results on the left, and the MLE results on the right for the pixels corresponding to the high intensity regions in the image. The statistical parameters for the SD histograms are shown on the plots. It is observed that the two methods of reconstruction do not show much difference in the high intensity regions. Figure 10 shows the corresponding sets of histograms for the low intensity regions within the brain phantom. The difference between the FBP and MLE methods is quite evident, with a substantial decrease in the variance of the MLE results. Finally, Fig. 11 shows the corresponding histograms for the low intensity regions inside and outside the brain, including the pixels outside the brain phantom, which, in principle, should not have any counts. The difference between the two methods of reconstruction is very marked.

It is interesting to show the "variance images", i.e., images whose pixel intensity is proportional to the SD of the 10 image pixels with respect to their mean. Figure 12 shows on the lef,t the variance image for the FBP reconstructions and, on the right, the corresponding image for the MLE reconstruction. The FBP image shows no significant features, in agreement with a variance which is uniform in both the high and low intensity regions within the phantom. The MLE image, however, shows a very clear structure, corresponding to the findings of smaller variance in the less intense regions of the phantom.

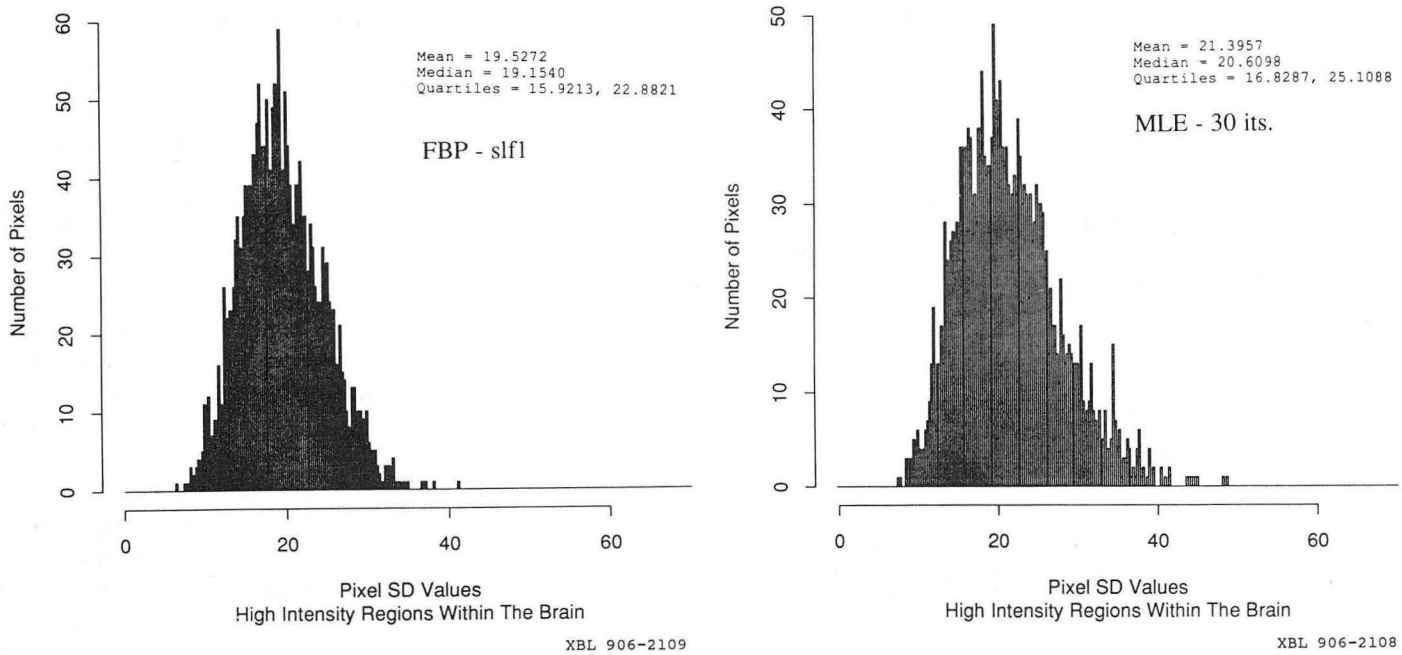

Fig. 9: Histogram of number of pixels having a certain Standard Deviation vs. Standard Deviation for the 1M reconstructions. Representative FBP results appear on the left, MLE results on the right.

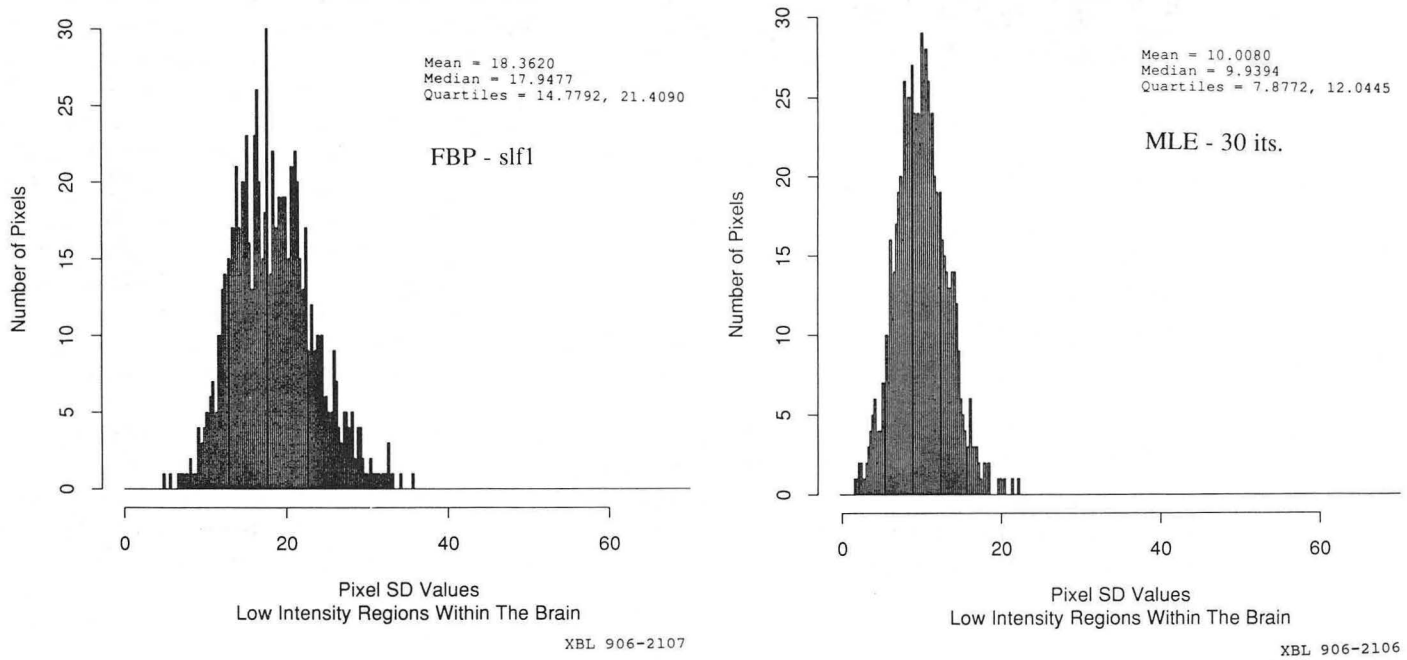

Fig. 10: SD Histograms for 1M reconstructions, FBP on the left, MLE on the right.

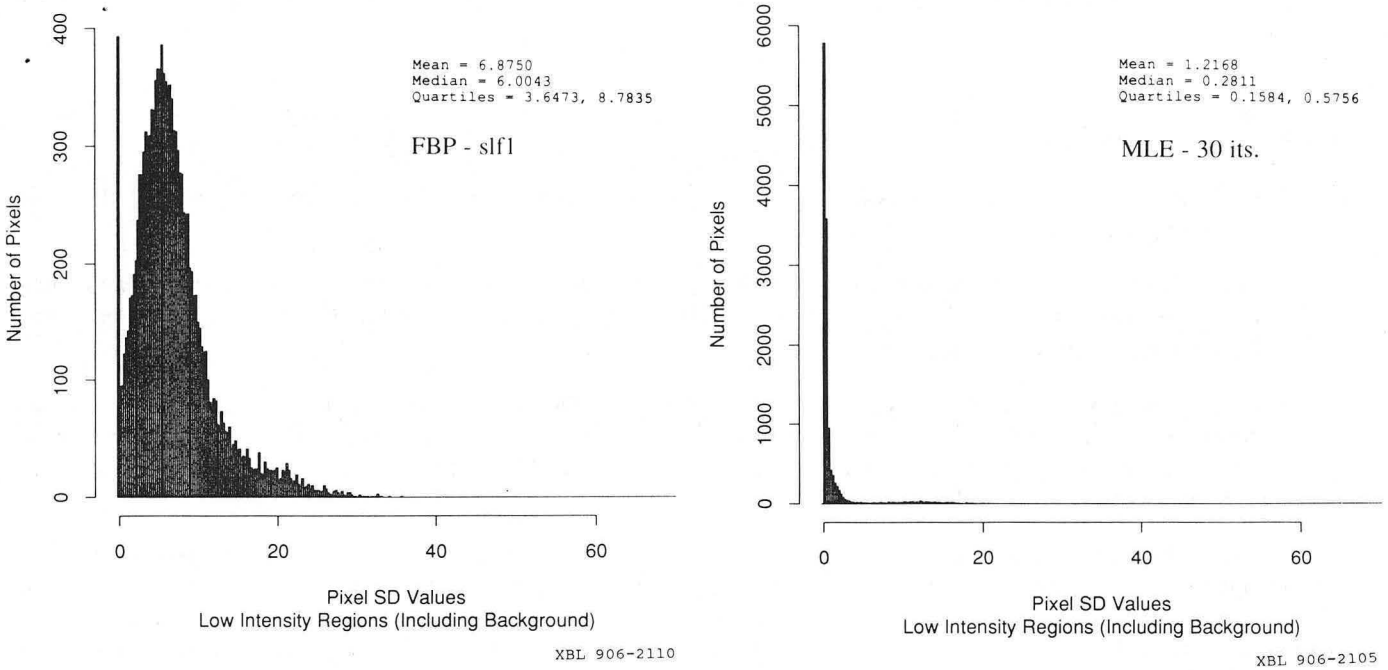

Fig. 11: SD Histograms for 1M reconstructions. The histograms include the region outside the brain phantom, where there are no expected counts.

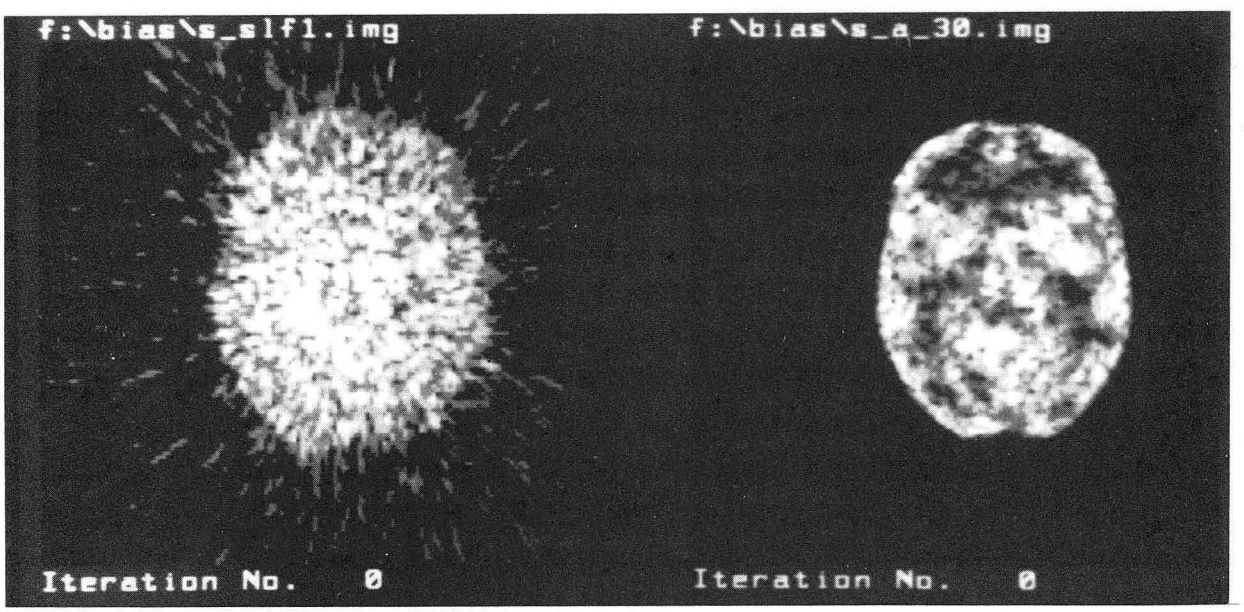

XBB 906-4732

Fig. 12: SD images for the FBP, left and MLE, right, from the 10 independent 1M count reconstructions.

The fact that the variance decreases when the number of counts in a region decreases appears to indicate that the utilization of the Poisson distribution in the statistically based reconstructions, in contrast to the implicit Gaussian assumption of the FBP, is causing the better results. It would be interesting to test whether an EM algorithm based on a Gaussian distribution, with a positivity constraint, would also give better results.

6. CONCLUSIONS

The analysis of image frequency spectra, bias and variance presented above give some indications as to what is "superior" about statistically based reconstruction algorithms in contrast to FBP for the Emission Tomography problem:

1) By chosing feasible images, statistically based algorithms provide images that can be sharper than FBP images without paying a significant penalty in noise.

2) The use of feasible MLE images obtained by iterating the EM algorithm past the onset of feasibility and filtering slightly results in images with no more bias than FBP images. Similar good results can be obtained by using the Bayesian algorithm with entropy prior.

3) Feasible images obtained by any of the acceptable statistically based methods have lower variance in the regions of lower intensity than the FBP images. Lesions in those regions should be more detectable and the time variation of isotope uptake in regions other than the more intense regions should be more accurate when obtained from statistically based reconstructions.

We feel that the above study places us in the position to initiate an ROC study in an appropriate collaboration with some knowledge of what we can attempt to prove. It will be interesting to see how the advantages described above translate themselves at the time of carrying out a medical diagnostic. It is interesting to note that FDG studies are likely to benefit less from statistically based reconstruction methods than other studies. FDG brain studies will always contain lesions (hotter or colder than the surroundings) in areas with a substantial number of counts. Other kinds of studies in which one wants to observe and/or measure low activity features in cold surroundings, even in the presence of hot areas elsewhere, should take better advantage of the lower variance characteristics of the statistically based reconstructions.

7. ACKNOWLEDGMENTS

The authors would like to acknowledge stimulating discussions with Peter Bickel, Deborah Nolan, Eugene Veklerov and Jorge Nunez during the course of this work. This work has been supported, in part, by a grant from the National Institutes of Health, CA-39501 and by the Director, Office of Energy Research, Office of Health and Environmental Research, Physical and Technological Division, of the U.S. Department of Energy under Contract No. DE-AC03-76SF00098.

8. REFERENCES

1. J. Llacer, E.l Veklerov and J. Nunez, "Statistically based image reconstruction for emission tomography," Intern. Journal of Imaging Systems and Tech., Vol 1, pp 132-148, 1989.

2. L.A. Shepp and Y. Vardi, "Maximum liklihood reconstruction for emission tomography," *IEEE Trans. Med. Imaging,*, vol. MI-1, pp. 113-122, 1982.

3. J. Llacer and E. Veklerov, "Feasible Images and practical stopping rules for iterative algorithms in emission tomography," *IEEE Trans. Med. Imaging,*, vol. MI-8, No. 2, pp. 186-193, 1989, and correction on vol. MI-9, No. 1, p.112, 1990.

4. J. Llacer, A. Chatterjee, H.C. Jackson, J.C. Lin and M.V. Zunzunegui, "An imaging instrument for positron emitting heavy ion beam injection," IEEE Trans. Nucl. Sci., Vol. NS-26, No. 1, pp. 634-647, 1979.

5. J. Llacer, A. Chatterjee, E.K.Batho and J.A. Poskanzer, "Design analysis and performance evaluation of a two-dimensional camera for accelerated positron emitter beam injection by computer simulation," IEEE Trans. Nucl. Sci., Vol. NS-30, No. 1, pp 617-625, 1983.

6. C.E. Floyd, R.J. Jaszczack and R.E.Coleman, "Inverse Monte Carlo: a unified reconstruction algorithm for PECT," IEEE Trans. Nucl. Sci., Vol. NS-32, No. 1, pp. 779-785, 1985.

7. E. Veklerov, J. Llacer and E.J. Hoffman, "MLE reconstruction of a brain phantom using a Monte Carlo transition matrix and a statistical stopping rule," IEEE Trans. Nucl. Sci., NS-35, No. 1, pp. 603-607, 1988.

8. E.J. Hoffman, A.R.Ricci, L.M.A.M. van der Stee and M. E. Phelps, "ECAT-III - Basic Design Considerations," IEEE Trans. Nucl. Sci., Vol. NS-30, No. 1, pp 729-733, 1983.

9. R.H. Huesman, G.T.Gullberg, W.L.Greenberg and T.F. Budinger, "Donner algorithms for reconstruction tomography," Lawrence Berkeley Laboratory Report No. 214, October 1977.

10. R. W. Hamming, Digital Filters, Prentice Hall, p. 189, 1977.

11. J. Llacer, E. Veklerov and J. Nunez, "The concept of causality (feasibility) in image reconstruction," NATO Advanced Study Institute, Povoa, Portugal, Sept. 1988, LBL Report 25877.

12. J. Nunez and J. Llacer, "A fast Bayesian reconstruction algorithm for emission tomography with entropy prior converging to feasible images," to be published in IEEE Trans. Med. Imaging, Vol. 9, No. 2, 1990.

13. D.L. Snyder, M.I. Miller, L.J. Thomas and D.A. Politte, "Noise and edge artifacts in maximum likelihood reconstructions for emission tomography," IEEE. Trans. Med. Imaging, MI-6, No. 3, pp. 228-238, 1987.

14. E. Veklerov and J. Llacer, "The feasibility of images reconstructed with the method of sieves," to be published in IEEE. Trans. Nucl. Sci., Vol 37, No. 2, 1990.

LAWRENCE BERKELEY LABORATORY
TECHNICAL INFORMATION DEPARTMENT
1 CYCLOTRON ROAD
BERKELEY, CALIFORNIA 94720